

## X-ray and HRTEM structure analysis of orientite

MARCELLO MELLINI, STEFANO MERLINO, AND MARCO PASERO

*Dipartimento di Scienze della Terra dell'Università di Pisa and  
C.N.R., C.S. Geologia Strutturale e Dinamica dell'Appennino  
via S. Maria 53, 56100 Pisa, Italy*

### Abstract

Orientite is orthorhombic,  $a = 9.044(10)$ ,  $b = 6.091(7)$ ,  $c = 19.031(20)$  Å, with ideal crystal chemical formula  $\text{Ca}_8\text{Mn}_{10}^{3+}[(\text{SiO}_4)_3(\text{Si}_3\text{O}_{10})_3(\text{OH})_{10}]\cdot 4\text{H}_2\text{O}$  in the unit cell. A structural model for orientite was proposed on the basis of chemical data, X-ray and HRTEM (High Resolution Transmission Electron Microscopy) analyses. The model was refined to  $R = 0.069$ , using 650 independent reflections collected with  $\text{MoK}\alpha$  radiation. The structure is characterized by the regular alternation in the  $c$  direction of two distinct structural modules; an “ardennite” module is built up from  $(\text{SiO}_4)$ ,  $(\text{Si}_3\text{O}_{10})$  and  $(\text{MnO}_6)$  groups, and the other module is built up from  $(\text{Si}_3\text{O}_{10})$  groups and water molecules; calcium cations fill the cavities and are linked to seven oxygen atoms.

HRTEM not only demonstrated the occurrence of faulted sequences, and a new polytypic variant with 38 Å  $c$  periodicity, but also was extremely valuable in assessing the most likely structure model for orientite.

Finally, a characteristic feature of orientite is the extensive occurrence of microvoids, elongated in the  $c$  direction, and located at the borders between misfitting crystal regions.

### Introduction

Orientite is a basic calcium and manganese (III) silicate. It occurs as a low temperature replacement mineral in alumina-poor manganese oxide and oxysalt ore bodies. The mineral was first reported from Oriente Province, Cuba, by Hewett and Shannon (1921), and its optical crystallography was later revised by Sclar (1961). Moore (1965) first stressed the crystallographic relationships between orientite and ardennite,  $\text{Mn}_8^+\text{Al}_{12}[(\text{AsO}_4)_2(\text{SiO}_4)_4(\text{Si}_3\text{O}_{10})_2(\text{OH})_{12}]$ , at a time when the crystal structure of ardennite (Donnay and Allmann, 1968; Allmann and Donnay, 1971) was not yet known. More recently, Moore et al. (1979) described a second occurrence of orientite from Keweenaw County, Michigan.

Up to now, two different structure models for orientite have been proposed: the MM model of Mellini and Merlino (1982) and the MSA model of Moore, Shen and Araki (Moore et al., 1985). In the present paper we present and support a third model, MMP, intermediate between the MM and the MSA structures. Furthermore, evidence of the structural disorder in orientite is presented.

### Models for the orientite structure

Moore et al. (1985) presented a comprehensive appraisal of the chemical and structural relationships within the family of  $6 \times 9$  Å modular sheet structures. Many minerals comprise this group, including chloritoid, lawsonite, sursassite, macfallite, pumpellyite, pumpellyite- $(\text{Mn}^{2+})$ , julgoldite, ardennite, orientite, ruizite, santafeite and bermanite. All of them have two lattice parameters that are 6 and 9 Å long, while the third parameter varies

from mineral to mineral. All these structures can be built starting from  ${}_2^{\infty}[\text{M}_2^+\Phi_2(\text{TO}_4)_2]$  sheets, where M is an octahedrally coordinated cation and  $\Phi$  is usually hydroxyl. Successive sheets sandwich variable intersheet material, which consists of both octahedral and tetrahedral coordination polyhedra.

On the basis of such an approach, Moore et al. (1985) proposed for orientite a structural model in which adjacent  ${}_2^{\infty}[\text{M}_2^+\Phi_2(\text{TO}_4)_2]$  sheets are connected through additional  $\text{SiO}_4$  tetrahedra, and this connection gives rise to  $\text{Si}_3\text{O}_{10}$  groups (Fig. 1a, hereafter called the MSA model). It seems convenient to remark that Moore et al. (1985) were aware of the disordered nature of orientite, and assumed that the central tetrahedral site had only partial occupancy, the corresponding  $\text{SiO}_4$  sheets in the structure being partly substituted by sheets of half-occupied manganese octahedra. The MSA model has space group  $Ccmm$  in the unit cell setting of Figure 1a. In what follows we shall always refer to such a setting, with the  $c$  axis indicating the direction along which the sheets are stacked and the  $b$  axis indicating the direction of the edge-sharing octahedral chains. A different setting was assumed by Moore et al. (1985), with space group  $Bbmm$ , and it transforms to the present one by the  $[\bar{1}00/001/010]$  matrix. The ideal unit cell content for the MSA model was  $\text{Ca}_8\text{Mn}_8^{3+}(\text{Si}_3\text{O}_{10})_4(\text{OH})_8\cdot 8\text{H}_2\text{O}$ .

A different model, MM, was previously proposed by Mellini and Merlino (1982), who developed it starting from the structural relationships existing between sursassite and pumpellyite. Sursassite,  $\text{Mn}_4^+\text{Al}_6[(\text{OH})_6(\text{SiO}_4)_2(\text{Si}_2\text{O}_7)_2]$ , and pumpellyite,  $\text{Ca}_4\text{Al}_6[(\text{OH})_6(\text{SiO}_4)_2-$

(Si<sub>3</sub>O<sub>7</sub>)<sub>2</sub>], apart from the different chemical contents, are built up from identical structural layers repeated according to different stacking sequences. The distinctive feature in the two structures lies in the different ways by which successive layers connect with each other through the octahedral sheets: whereas in pumpellyite similar silicate groups (ortho-ortho and diortho-diortho) face each other, in surassite different groups (ortho and diortho) face each other on the two sides of the octahedral sheets (Mellini et al., 1984). Similarly, ardennite, Mn<sub>8</sub><sup>3+</sup>Al<sub>12</sub>[(AsO<sub>4</sub>)<sub>2</sub>(SiO<sub>4</sub>)<sub>4</sub>(Si<sub>3</sub>O<sub>10</sub>)<sub>2</sub>(OH)<sub>12</sub>], is characterized by orthosilicate and trisilicate groups, with different groups facing each other (Fig. 1b). By analogy with the sursassite–pumpellyite structures, a different structural modification for orientite was envisaged in the MM model, with similar groups facing each other (Fig. 1c). It has space group *Pcmm*, whereas *Pnmm* is the space group for ardennite. The ideal unit cell content for this MM model was Ca<sub>8</sub>Mn<sub>12</sub><sup>3+</sup>[(SiO<sub>4</sub>)<sub>6</sub>(Si<sub>3</sub>O<sub>10</sub>)<sub>2</sub>(OH)<sub>12</sub>].

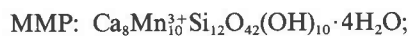
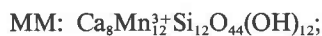
The MM and the MSA models differ only in the structural slabs between  $z = 0.18$  and  $z = 0.32$ , and between  $z = 0.68$  and  $z = 0.82$ . In the MSA model these slabs consist of silicate tetrahedra and water molecules, whereas in the MM model they contain edge-sharing Mn<sup>3+</sup> octahedra, with silicate tetrahedra attached on the two sides of the octahedral chains. As a consequence, the two models differ also in chemical composition, with MSA and MM containing respectively eight and twelve octahedral cations per unit cell.

The recalculation of the chemical analyses of orientite from Cuba (Hewett and Shannon, 1921) and from Keweenaw County (Moore et al., 1979) pointed to the presence of ten octahedral cations per unit cell. These chemical data, and the still more compelling evidence from our HRTEM study of the mineral, prompted us to develop a third model, MMP, depicted in Figure 1d. This model has space group *P2mm* and is characterized by regular alternation of MM and MSA structural slabs; correspondingly, its ideal chemical formula, intermediate between the MM and MSA formulae, is Ca<sub>8</sub>Mn<sub>10</sub><sup>3+</sup>[(SiO<sub>4</sub>)<sub>5</sub>(Si<sub>3</sub>O<sub>10</sub>)<sub>3</sub>(OH)<sub>10</sub>]·4H<sub>2</sub>O.

It should be noted that the three models present the same scaffolding of oxygen atoms and differ only in the locations of tetrahedral and octahedral cations in the slabs between  $z = 0.18$  and  $z = 0.32$  and between  $z = 0.68$  and  $z = 0.82$ . Therefore, the three models are expected to produce very similar X-ray diffraction patterns, characterized by a common distribution of the strongest reflections, as all of them simulate a common *Ccmm* super-symmetry.

#### Chemical data

The three models discussed above present structural differences that are reflected by their chemical composition; in fact the ideal crystal chemical formulae for them are as follows:



The models are thus chemically related by successive removal of two MnO(OH) units per unit cell and corresponding introduction of four water molecules.

These ideal formulae can be compared with the actual unit cell contents of orientite from Keweenaw County and Oriente Province, obtained from the chemical data of Moore et al. (1979) and Hewett and Shannon (1921), respectively, on the basis of 56(O + OH + H<sub>2</sub>O): Keweenaw County: Ca<sub>7.84</sub>(Mn<sub>8.25</sub><sup>3+</sup>Mg<sub>0.25</sub>Cu<sub>0.56</sub><sup>2+</sup>)<sub>tot=10.06</sub>(Si<sub>11.27</sub>V<sub>0.23</sub>S<sub>0.27</sub>)<sub>tot=11.77</sub>O<sub>42</sub>(OH)<sub>8.9</sub>·5.1H<sub>2</sub>O; Oriente Province (average of three analyses): Ca<sub>8.5</sub>(Mn<sub>8.77</sub><sup>3+</sup>Al<sub>0.45</sub><sup>3+</sup>Fe<sub>0.43</sub><sup>3+</sup>Mn<sub>0.28</sub><sup>2+</sup>)<sub>tot=9.93</sub>Si<sub>11.60</sub>O<sub>42</sub>(OH)<sub>9.1</sub>·4.9H<sub>2</sub>O.

The chemical data thus support the MMP model. As regards orientite from Keweenaw County, the calculated density of 3.36 g cm<sup>-3</sup> compares well with the observed value 3.33 g cm<sup>-3</sup>. The vanadium cations probably substitute for silicon cations in the Si4 site, which corresponds to the (As,V) site in ardennite. The presence of copper, an element that is infrequently so abundantly present as a minor component in silicate minerals, may be easily explained by the distortion of the Mn<sup>3+</sup> coordination polyhedra through the Jahn-Teller effect exhibited by Mn<sup>3+</sup> cations in high spin configuration: in these sites Cu<sup>2+</sup> cations, which similarly display the Jahn-Teller effect, find a suitable environment.

As regards the Oriente Province specimen, the calculated density of 3.35 g cm<sup>-3</sup> is markedly higher than the measured value of 3.15(4) g cm<sup>-3</sup> (Moore et al., 1979). It is possible that the black opaque pigment that covers the orientite crystals from Oriente Province (Hewett and Shannon, 1921) prevented reliable determination of the density. In the chemical analysis of the material from Oriente Province by Hewett and Shannon (1921), vanadium, sulphur and copper were not determined. However, we observed the presence of vanadium and sulphur, roughly 0.2 and 0.1 atoms per cell, respectively, also in the Oriente Province specimen, with TEM/EDS (Energy Dispersive Spectrometry). Moreover, we cannot exclude the presence of copper in this specimen, as the copper X-ray lines are usually observed as an artifact under TEM/EDS conditions, due to copper support grids and copper in the goniometer specimen holder.

#### X-ray structure analysis

The X-ray diffraction study was carried out using a crystal of orientite from Oriente Province and selected using Weissenberg photographs. Intensity data were collected by a Philips PW1100 single crystal automatic diffractometer, using MoK $\alpha$  radiation. The parameters of the orthorhombic unit cell are  $a = 9.044(10)$ ,  $b = 6.091(7)$ ,  $c = 19.031(20)$  Å. The true unit cell is primitive, although reflections with  $h + k = 2n$  are much more intense than reflections with  $h + k = 2n + 1$ , thus indicating a pseudo *C*-centering. Most  $0kl$  reflections were absent for  $l = 2n + 1$ , but some of them, although weak, were observed, and

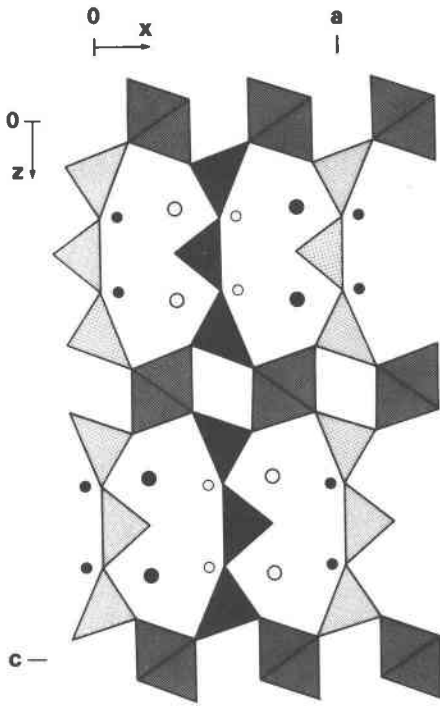
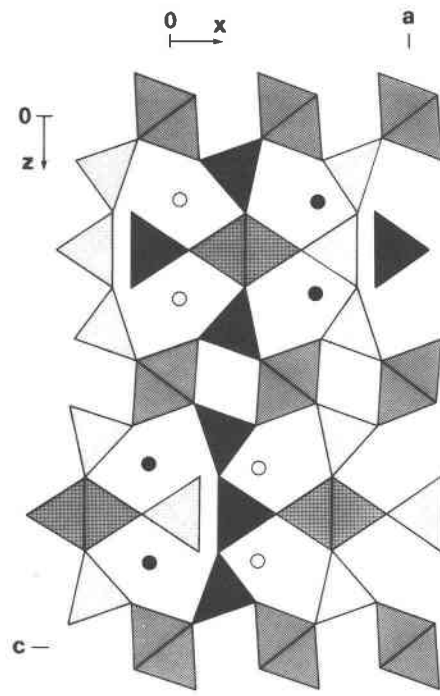
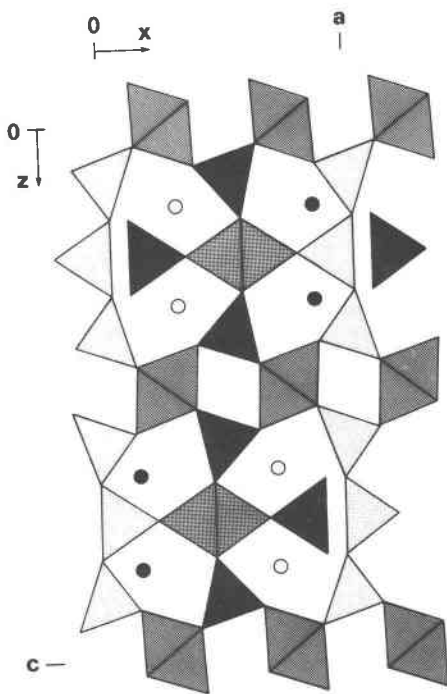
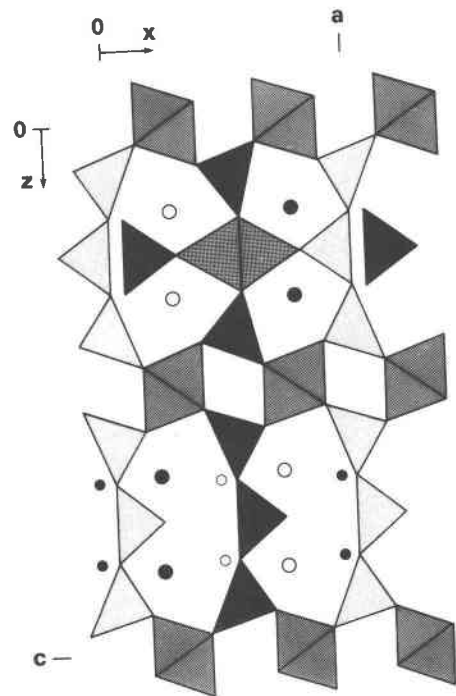
**a****b****c****d**

Table 1. Final atomic positions and isotropic temperature factors, *B*. O is site occupancy and *M* is site multiplicity

Site	O	M	x	y	z	B	Site	O	M	x	y	z	B
Ca1	1.0	0.5	0.2876	1/2	0.1608(4)	0.39(11)	01	1.0	1.0	0.3788(15)	0.2143(27)	0.0791(8)	0.62(26)
Ca2	1.0	0.5	0.8136(7)	0	0.1569(4)	0.75(12)	02	1.0	1.0	0.8691(14)	0.2886(24)	0.0781(7)	0.30(24)
Ca3	1.0	0.5	0.7093(8)	1/2	0.6571(4)	1.38(13)	03	1.0	0.5	0.1394(26)	1/2	0.0616(13)	1.25(42)
Ca4	1.0	0.5	0.1836(7)	0	0.6578(4)	0.36(11)	04	1.0	0.5	0.6301(21)	0	0.0579(11)	0.06
Mn1	1.0	1.0	0.2560(3)	0.2511(6)	0.0018(2)	0.19(5)	05	1.0	0.5	0.2932(25)	0.2383(53)	1/4	1.64(42)
Mn2	0.84	0.5	0.5507(5)	0.2488(11)	1/4	0.06	06	1.0	0.5	0.7910(22)	0.2840(40)	1/4	0.74(38)
Mn3	1.0	1.0	0.7511(3)	0.2591(7)	-0.0028(2)	0.47(6)	07	1.0	0.5	0.5599(23)	0	0.1779(11)	0.36(37)
Si1	1.0	0.5	-0.0256(11)	1/2	0.0934(6)	1.12(17)	08	1.0	0.5	0.0110(26)	1/2	0.1810(13)	1.02(44)
Si2	1.0	0.5	0.4763(9)	0	0.1006(5)	0.06	09	1.0	0.5	0.0694(28)	0	0.1799(14)	1.62(48)
Si3	0.84	0.25	-0.1026(16)	1/2	1/4	0.06	10	1.0	0.5	0.1301(23)	0	0.0247(11)	0.56(36)
Si4	0.84	0.25	0.1949(14)	0	1/4	0.37(20)	11	1.0	0.5	0.6409(21)	1/2	0.292(11)	0.06
Si5	1.0	0.5	0.0454(9)	1/2	0.5963(4)	0.06	12	1.0	0.5	0.5284(31)	1/2	0.1806(16)	2.14(55)
Si6	1.0	0.5	0.5258(9)	0	0.5971(5)	0.25(14)	13	1.0	1.0	0.6270(13)	0.2137(25)	0.5877(7)	0.19(23)
Si7	1.0	0.25	0.1197(11)	1/2	3/4	0.42(16)	14	1.0	1.0	0.1289(16)	0.2615(33)	0.5807(8)	1.07(27)
Si8	0.68	0.25	0.6029(40)	0	3/4	4.38(79)	15	1.0	0.5	-0.1165(25)	1/2	0.5604(13)	1.08(43)
Mn2A	0.16	0.5	0.0691(40)	0.2295(79)	1/4	1.41(67)	16	1.0	0.5	0.3778(22)	0	0.5515(12)	0.42(36)
Si3A	0.16	0.25	0.3929(82)	0	1/4	0.06	17	1.0	0.5	0.1954(23)	0.2537(48)	3/4	0.93(38)
Si4A	0.16	0.25	0.6936(72)	1/2	1/4	0.06	18	1.0	0.5	0.4813(22)	0	0.6834(11)	0.06
Mn2B	0.32	0.5	0.4615(15)	0.2534(31)	3/4	0.49(23)	19	1.0	0.5	0.0060(22)	1/2	0.6768(11)	0.40(37)
Si4B	0.32	0.25	0.7956(42)	0	3/4	1.00(63)	20	1.0	0.5	0.8617(21)	0	0.5410(11)	0.06
							21	1.0	0.5	0.3773(26)	1/2	0.5268(13)	1.10(45)
							22	1.0	0.5	0.7054(20)	0.2104(35)	3/4	0.05(34)
							23	1.0	0.5	-0.0782(29)	0	0.6799(15)	2.01(53)
							24	1.0	0.5	0.4300(25)	1/2	0.6771(13)	0.72(42)

this casts some doubt on the strict validity of the *c* glide symmetry. Whereas these observations definitely rule out the MSA model, which requires *Ccmm* symmetry, we preferred to refine both MM and MMP models, which have *Pcmm* and *P2mm* space groups. Using 650 reflections with  $F_o > 2\sigma F_o$ , the following reliability indices were found: 0.135 for the MM and 0.095 for the MMP model. Whereas the refinement proceeded quite smoothly for the MM model, difficulties were met in refining the MMP model. In the latter case the corresponding parameters of atoms related by the *c* pseudo-glide showed high correlation coefficients. The refinement was therefore concluded for the MMP model according to the suggestions by Rae (1974). Distinct maxima were found in a difference Fourier synthesis, calculated after several refinement cycles, and they seemed to indicate the occurrence of structural disorder. The disorder scheme was interpreted, atoms with partial occupancy were introduced, and, as a consequence, the occupancies of other atoms already located were lowered. In this way, the refinement was carried out to a final *R* value of 0.069. The final atomic positions and isotropic temperature factors are given in Table 1.<sup>1</sup>

Table 1 presents, in addition to all the atoms of the MMP model, five more atomic positions, Mn2A, Si3A, Si4A with 0.16 occupancy and Mn2B, Si4B with 0.32

occupancy. If we consider the three first atomic positions, together with the 0.84 partial occupancy for the Si3, Si4 and Mn2, we can infer that such a distribution scheme corresponds to the displacement of the whole structural slab between  $z = 0.18$  and  $z = 0.32$ , with  $\frac{1}{2}(\mathbf{a} + \mathbf{b})$  as displacement vector. Such a feature is completely consistent with the stacking faults we observed by TEM and later described. As regards the two other additional atoms, Mn2B and Si4B, their introduction, together with the 0.68 occupancy for Si8, corresponds to substituting a chain of manganese octahedra with a connected (SiO<sub>4</sub>) tetrahedron to the central Si8 tetrahedron in the trisilicate group. This substitution gives rise to domains with the MM structure besides the more abundant domains with the MMP structure.

The refinement was carried out also for the MM model in the space group *Pcmm*. Also in this case the difference Fourier synthesis revealed additional maxima, which were introduced with variable occupancy in the least squares refinement process. The final *R* value, obtained with the same 650 reflections, was 0.085; according to the Hamilton test (Hamilton, 1965), the hypothesis that the MM model describes the structure of orientite more correctly than the MMP model does can be rejected at the 0.005 level.

The crystal structure of orientite is described in Figure 2 in terms of the main constituent units: chains of edge-sharing Mn<sup>3+</sup> octahedra run along [010] and are connected by (SiO<sub>4</sub>) orthosilicate and (Si<sub>3</sub>O<sub>10</sub>) trisilicate groups. The orthosilicate and trisilicate groups are stippled in Figure

<sup>1</sup> To obtain a copy of the  $F_o-F_c$  tables order Document AM-86-295 from the Business Office, Mineralogical Society of America, 1625 I Street, N.W., Suite 414, Washington, D.C. 20006. Please remit \$5.00 in advance for the microfiche.

Fig. 1. (a) MSA model for orientite, as seen along [010]; different grey tones indicate different *y* levels; larger circles are calcium cations, smaller circles are water molecules; (b) Crystal structure of ardenite, as seen along [010]; (c) MM model for orientite; (d) MMP model for orientite.

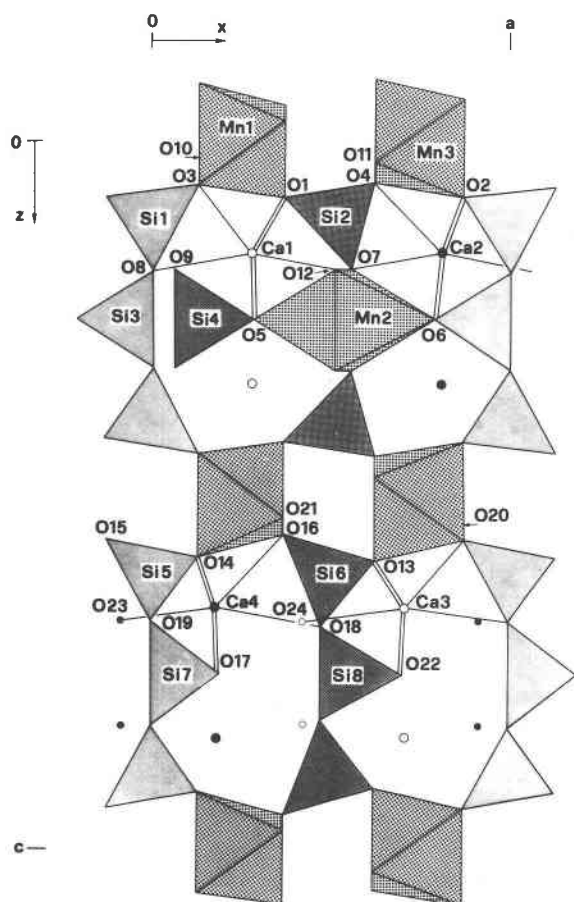
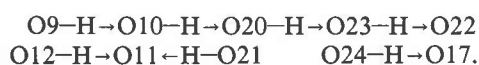


Fig. 2. Crystal structure of orientite as seen along [010].

2 by different tones of grey to indicate their different  $y$  levels. Four independent calcium cations, Ca1 and Ca3 on the mirror plane at  $y = 0$ , and Ca2 and Ca4 on the mirror plane at  $y = \frac{1}{2}$ , are linked to seven oxygen atoms. Table 2 reports the main bond distances in orientite together with the mean bond lengths in the various polyhedra. It was prepared by considering only the atoms corresponding to the MMP model. The values appear normal, apart from the distances in the Si4 tetrahedron, which corresponds to the (As,V) tetrahedral site in the structure of ardenite (Donnay and Allmann, 1968). Some vanadium substitution in this site may explain the anomalously large bond distances; this is in keeping with the results of the chemical analysis of the Keweenaw County specimen (Moore et al., 1979) and our TEM/EDS analysis on the Oriente Province specimen. The three independent octahedral sites possess a common distortion which is due to the marked Jahn-Teller effect for high spin  $Mn^{3+}$  cations: the coordination is a tetragonal bipyramid, with four shorter and two longer  $Mn^{3+}$ -O distances. The mean distance for the four short bonds is 1.93 and 1.94 Å for the Mn1 and Mn3 sites, as found in ruizite and macfallite (Moore et al., 1985) and bermanite (Kampf and Moore, 1976), and is 2.04 Å for the Mn2 site.

Table 2 also gives the  $O \cdots O$  distances between oxygen atoms not linked to the same cation and shorter than 3.10 Å. A hydrogen bond system may be suggested on the basis of these data and of a valence balance calculation computed assuming the ideal composition  $Ca_8Mn_{10}^{3+}Si_{12}O_{42}(OH)_{10} \cdot 4H_2O$ . The calculations, following Brown and Wu (1976), support the MMP structural model for orientite, which indicates ten hydroxyl anions and four water molecules in the unit cell. We suggest the following hydrogen bond system as the most probable:



In this scheme O9, O10, O12, O20 and O21 are hydroxyl anions and O23 and O24 water molecules. O23 lies on the mirror plane at  $y = 0$  and forms two hydrogen bonds with two equivalent O22 atoms lying on the opposite sides of the mirror plane. Similarly, O24 forms two hydrogen bonds with two equivalent O17 atoms on the opposite sides of the mirror plane at  $y = \frac{1}{2}$ .

#### HRTEM structure analysis

The HRTEM analysis was conducted on both the Oriente Province and Keweenaw County specimens. Crystal powders were examined with a Philips 400T microscope, according to standard procedures (e.g., Mellini et al., 1984). Images were interpreted by comparison with image simulations, obtained with the SHRLI set of programs (O'Keefe and Buseck, 1979).

Most of the structure models of Figure 1 consist of structural slabs, 9.5 Å thick and repeated along [001] by glide planes. The least symmetric arrangement occurs only in the MMP model of Figure 1d. In this model, slabs consisting only of  $(Si_3O_{10})$  groups alternate with different, ardenite-like slabs consisting of both  $(Si_3O_{10})$  groups and tetrahedral/octahedral clusters. The symmetry features present in the ardenite, MM and MSA models obviously are present in the corresponding [010] computed images. These images therefore consist of [100] contrast rows that are repeated every 9.5 Å along [001] in enantiomorphic relationship by  $c$  or  $n$  glide planes. Whereas excellent fit occurs between the computation and the observations in the case of ardenite, no fit occurs when the orientite images are compared with the results from the MM and MSA models. In fact, the experimental orientite images do not show any 9.5 Å  $c$  subperiod but show marked 19 Å  $c$  period. At the best imaging conditions, two [100] strips having different contrast alternate along [001] every 9.5 Å. The first strip consists of white dots 9 Å apart along [100] (and this is not different from the MM or ardenite cases), but the second strip consists of a doubled population of white dots, now 4.5 Å apart. As a brief historical note, this observation led us to doubt both the MM and MSA models, prompted us to look for alternative models, and suggested the MMP model. This model resulted in similar observed and computed images (Fig. 3). It is interesting to recall what these white dots mean: in the [010]

Table 2. Selected interatomic distances (Å) in orientite

Ca1 - 01 (x2) 2.47(2)	Mn1 - 01 1.86(2)	Si2 - 01 (x2) 1.63(2)	Si8 - 018 (x2) 1.68(3)
- 03 2.31(3)	- 03 2.17(1)	- 04 1.61(2)	- 022 (x2) 1.58(3)
- 05 (x2) 2.33(2)	- 010 1.96(1)	- 07 1.65(2)	Average value 1.63
- 08 2.53(2)	- 014 1.95(2)	Average value 1.63	Average value 1.63
- 012 2.21(3)	- 016 2.14(2)		
Average value 2.38	- 021 1.95(2)		
	Average values 1.93 (x4)	Si3 - 06 (x2) 1.63(2)	
	2.16 (x2)	- 08 (x2) 1.67(3)	
		Average value 1.65	
Ca2 - 02 (x2) 2.36(2)	Mn2 - 05 2.33(2)		09 - 010 3.00(3)
- 04 2.51(2)	- 06 2.18(2)		010 - 020 2.73(3)
- 06 (x2) 2.48(2)	- 07 (x2) 2.05(2)	Si4 - 05 (x2) 1.70(3)	011 - 012 3.06(4)
- 07 2.33(2)	- 012 (x2) 2.03(2)	- 09 (x2) 1.75(3)	011 - 021 2.61(3)
- 09 2.35(3)	Average values 2.04 (x4)	Average value 1.73	017 - 024 2.95(3)
Average value 2.41	2.26 (x2)		020 - 023 2.70(3)
		Si5 - 014 (x2) 1.66(2)	021 - 024 2.90(3)
Ca3 - 013 (x2) 2.31(1)	Mn3 - 02 1.88(1)	- 015 1.62(2)	022 - 023 2.69(3)
- 015 2.42(3)	- 04 2.24(1)	- 019 1.57(2)	
- 019 2.71(2)	- 011 1.88(1)	Average value 1.63	
- 022 (x2) 2.50(2)	- 013 1.99(1)		01 - 011 3.09(2)
- 024 2.55(2)	- 015 2.19(2)	Si6 - 013 (x2) 1.60(1)	08 - 09 3.09(1)
Average value 2.47	- 020 2.00(1)	- 016 1.59(2)	013 - 021 3.08(2)
	Average values 1.94 (x4)	- 018 1.69(2)	014 - 020 2.99(2)
	2.22 (x2)	Average value 1.62	018 - 024 3.08(1)
Ca4 - 014 (x2) 2.22(2)	Si1 - 02 (x2) 1.63(2)		
- 016 2.68(2)	- 03 1.61(3)	Si7 - 017 (x2) 1.65(3)	
- 017 (x2) 2.34(2)	- 08 1.70(3)	- 019 (x2) 1.73(2)	
- 018 2.74(2)	Average value 1.64	Average value 1.69	
- 023 2.40(2)			
Average value 2.42			

images, they correspond, both in number and  $z$  coordinate, to the  $(\text{Si}_3\text{O}_{10})$  groups, whereas their  $x$  coordinate does not always coincide with the  $x$  coordinate of these groups, but shows  $\Delta x$  shifts depending on defocus and thickness.

Worsening of the imaging conditions (crystal misalign-

ment or imaging only the  $00l$  diffractions) produces poor two-dimensional images or one-dimensional lattice fringes. In this latter case, the MMP structure is expected to produce a well-defined 19 Å periodicity, whereas the ardenite, MM or MSA structures are expected to produce mainly 9.5 Å lattice fringes.

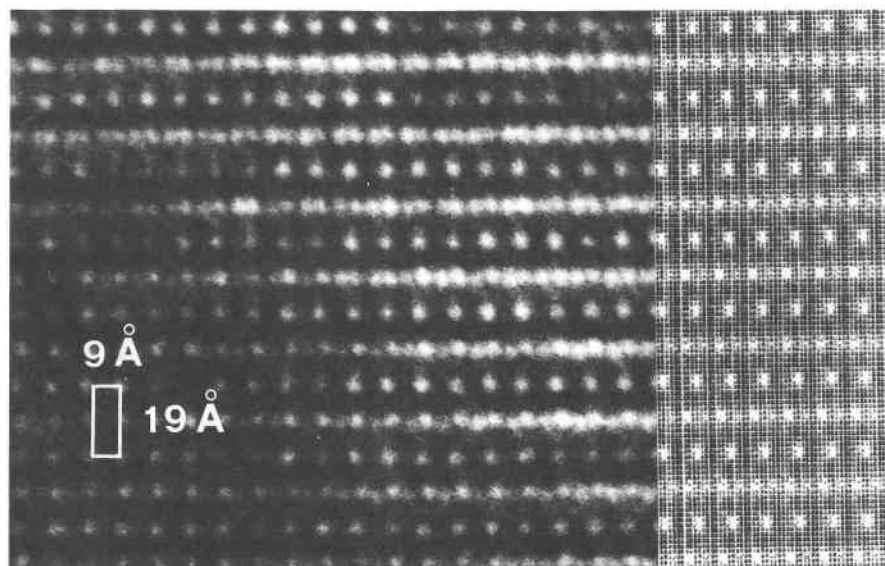


Fig. 3. [010] computed (MMP model, thickness 61 Å, defocus -200 Å) and observed lattice images for orientite.

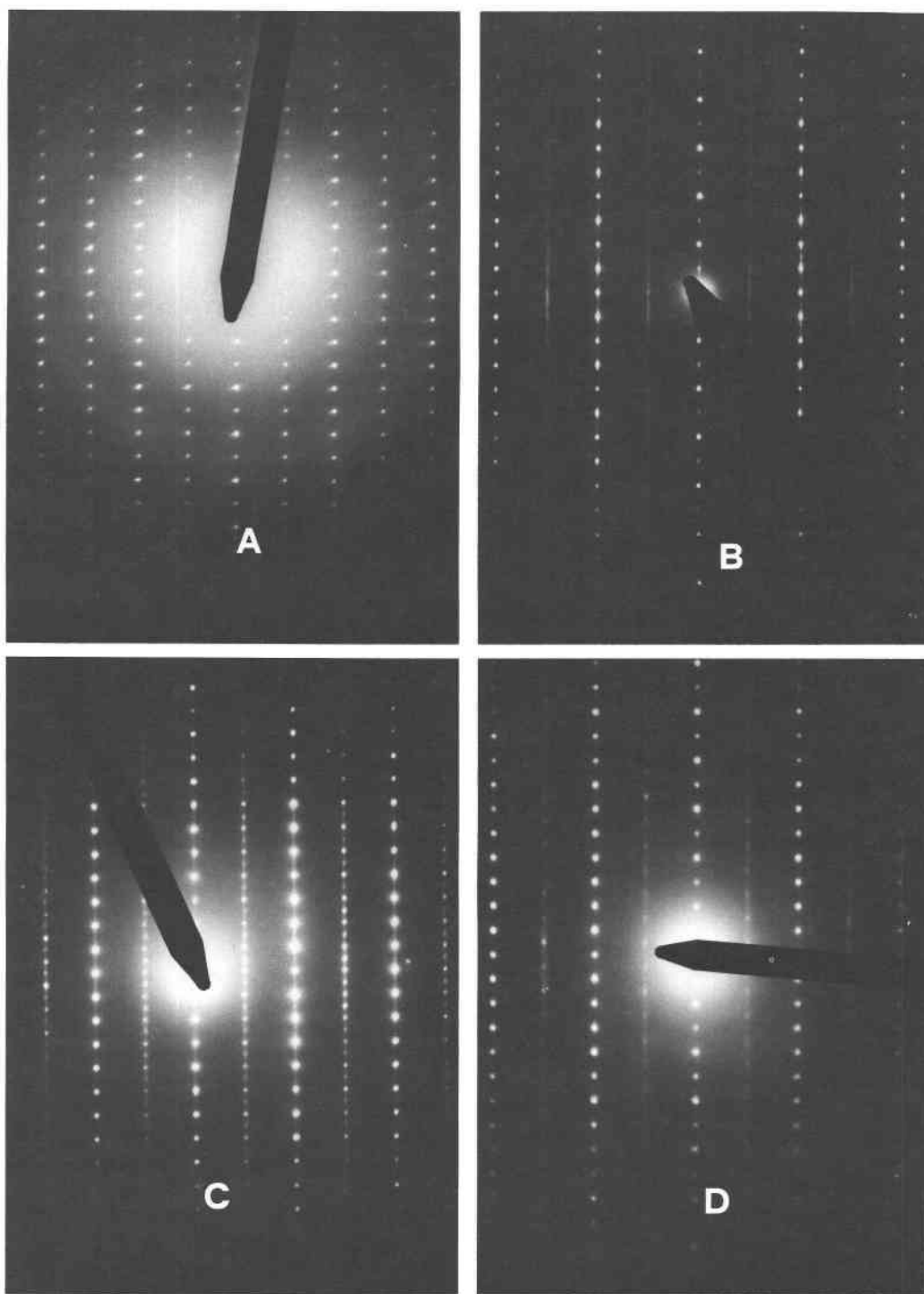


Fig. 4. Selected area [010] electron diffraction patterns for: (a) highly ordered orientite; (b) disordered orientite with diffuse odd- $h$  rows; (c) coexisting orientite and the 38 Å structure; (d) only the 38 Å structure.

#### The defect structure of orientite

##### Electron diffraction

Reciprocal space observations on orientite can be divided into four main types, although no sharp boundary limits these four groups:

(a) [010] SAD (Selected Area Diffraction) patterns consisting of sharp diffractions at positions that correspond to orientite reciprocal lattice points (Fig. 4a).  $00l$  spots with  $l = 2n + 1$  (which are kinematically forbidden in the  $C_{2mm}$  or  $P_{2mm}$  space groups of the MSA or MM model) are present.

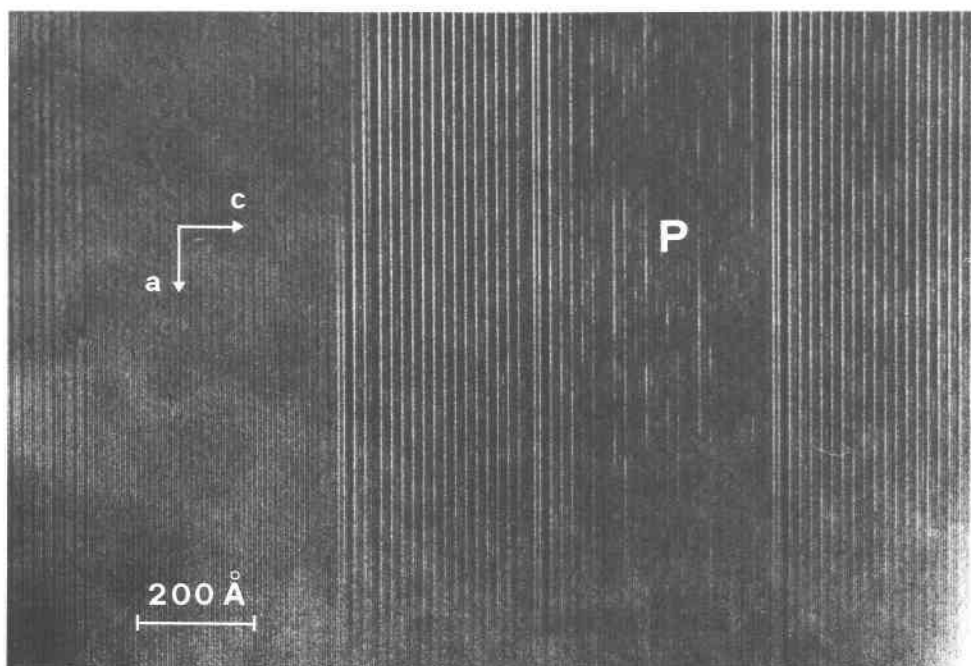


Fig. 5. Disordered alternation of (001) lamellae in orientite; different contrast patterns are evident; the P area shows more complex disorder.

(b) Patterns in which reciprocal lattice rows with  $h = 2n + 1$  (called odd- $h$  rows hereafter) are streaked in the  $c^*$  direction; their appearance spans from faint streaks with diffraction maxima in the expected positions to continuous streaks with no maxima at all (Fig. 4b).

(c) Patterns in which odd- $h$  rows have sharp spots, but the spot population along these rows is doubled. Besides the spots registered in the type (a) diffraction patterns ("orientite" spots), there are additional reflections that indicate a  $c$  period of 38 Å (Fig. 4c).

(d) Patterns in which the "orientite" spots in the odd- $h$  rows, which correspond to even  $l$  values when indexed on the basis of a 38 Å  $c$  parameter, are weak or absent; only the additional spots, corresponding to odd  $l$  values, are present, in some cases superimposed on weak diffuse streaks (Fig. 4d).

Whereas type (a) provides evidence for the existence of relatively large and ordered "orientite" regions, type (b) diffraction is indicative of extended disorder along [001]. Types (c) and (d) point to the existence of a new polytypic structure with a doubled  $c$  translation: type (d) diffraction patterns are due to this structure only, whereas type (c) diffraction patterns may be interpreted as due to the presence of domains of both orientite and the new structure. Lattice parameters for this structure are  $a = a_o$ ,  $c = 2c_o$  (the subscript "o" refers to the unit cell of orientite). If we reasonably assume that the new polytype results from a different stacking of "orientite" layers in the  $c$  direction, then we may infer that  $b = b_o$ . As discussed subsequently, the simplest polytypic variant corresponds to an  $I$ -centered cell, which is in keeping with the observed systematic

extinctions, in the type (d)  $h0l$  diffraction patterns, for  $h + l = 2n + 1$ .

#### Lattice imaging

Direct space observations confirm that orientite, from Keweenaw County as well as from Oriente Province, is

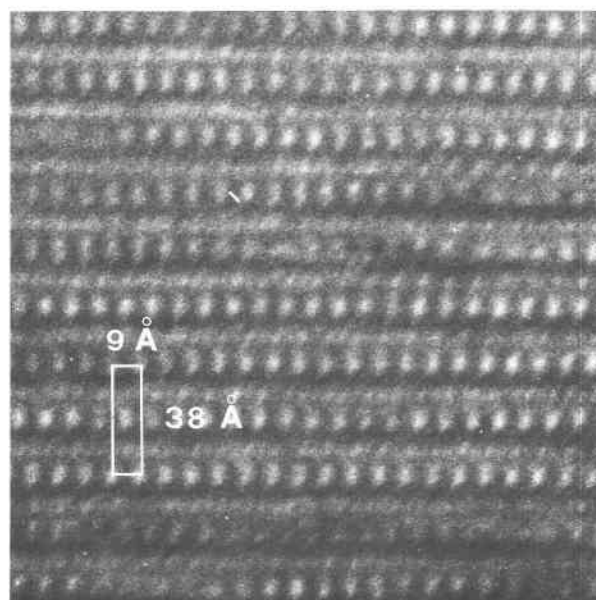


Fig. 6. HRTEM image of the ordered 38 Å polytype.

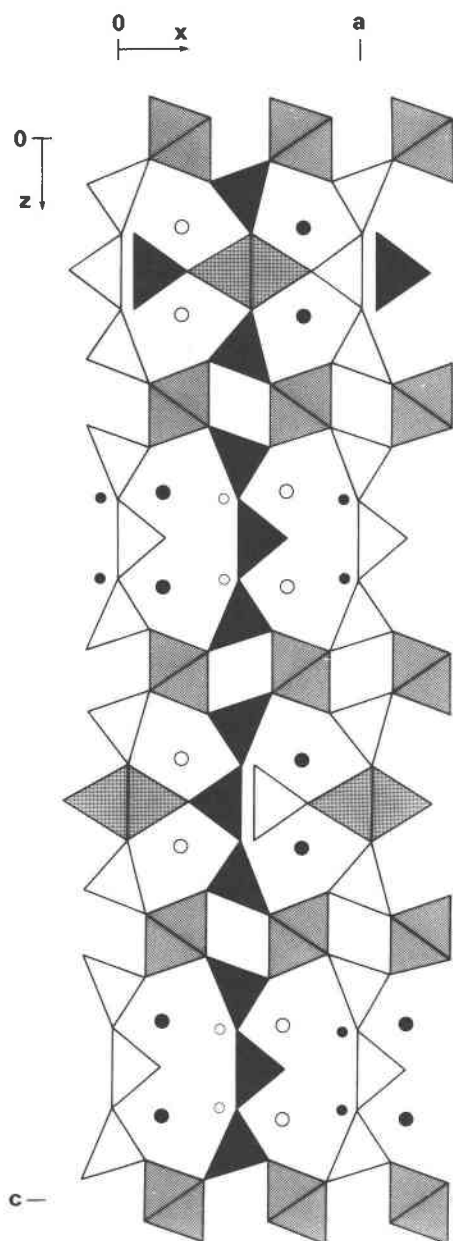


Fig. 7. Structure model for the 38 Å polytype.

characterized by abundant defect microstructures. The most frequent faults are due to the following: (a) intermixing of orientite *sensu stricto* with different, although closely related, structural arrangements; (b) frequent occurrence of the 38 Å polytype; (c) stacking faults; (d) microtubules and microvoids.

These microstructures are described in detail below.

(a) Intermixing typically involves (001) lamellar intercalation of different structures. All of them reveal a basic 9.5 Å, or 19 Å, period of lattice fringes. Faulting may consist either of thin isolated lamellae within a rather

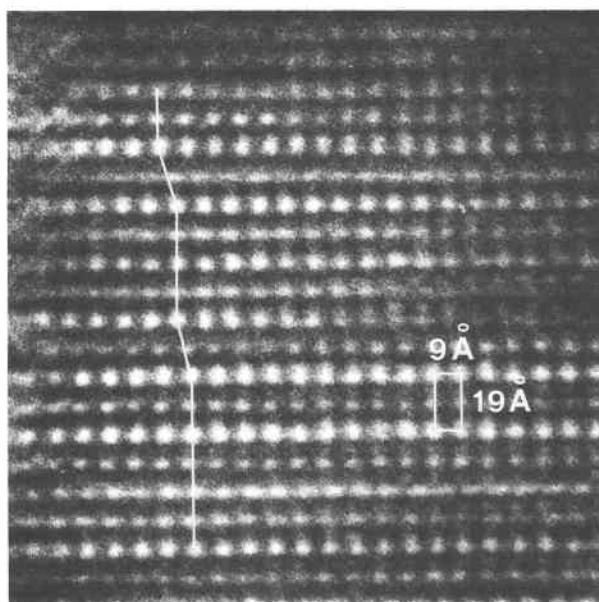


Fig. 8. Stacking faults in orientite, resulting from  $\frac{1}{2}(a_0 + b_0)$  fault vectors.

regular matrix or, as shown in Figure 5, may consist of faulted lamellae of greater thickness parallel to [001]. In this figure, three different lattice fringe systems appear. All of them display 19 Å periods but have different contrast patterns. Faulted lamellae with 9.5 Å period can be seen in several places, as well as lateral interruptions of the lattice fringes. In the region marked P, a complex patchy pattern dominates the simpler lamellar intergrowth which occurs elsewhere. Although these one-dimensional images cannot be straightforwardly interpreted in precise structural terms, it must be remarked that their periods, 9.5 and 19 Å, are related to the general topological arrangement of the orientite structure type, with its many possible modifications.

(b) The 38 Å polytype occurs in our specimens both as extended regions, some thousands of Å wide, of regular 38 Å structure (Fig. 6), and as fault structures intermixed with orientite. The lattice geometry indicated by the electron diffraction patterns as well as the HRTEM images point to a *B*- or *I*-centered cell for the 38 Å polytype. The *B* cell can be ruled out by taking into account the geometrical constraints that are valid for the whole family of the  $6 \times 9$  Å modular structures (namely, tetrahedral groups facing each other on both sides of the octahedral rows must be at the same *y* level). The proposed structural scheme for this *I*-centered polytype is given in Figure 7.

(c) The 38 Å polytype results from an ordered sequence of the orientite structural slabs, repeated according to the stacking vector  $c_0 + \frac{1}{2}(a_0 + b_0)$ . When applied in isolation, this vector gives rise to stacking faults, examples of which are given in Figure 8. Figure 9 is from a rather thick crystal (thickness greater than 150 Å) and shows occurrence of

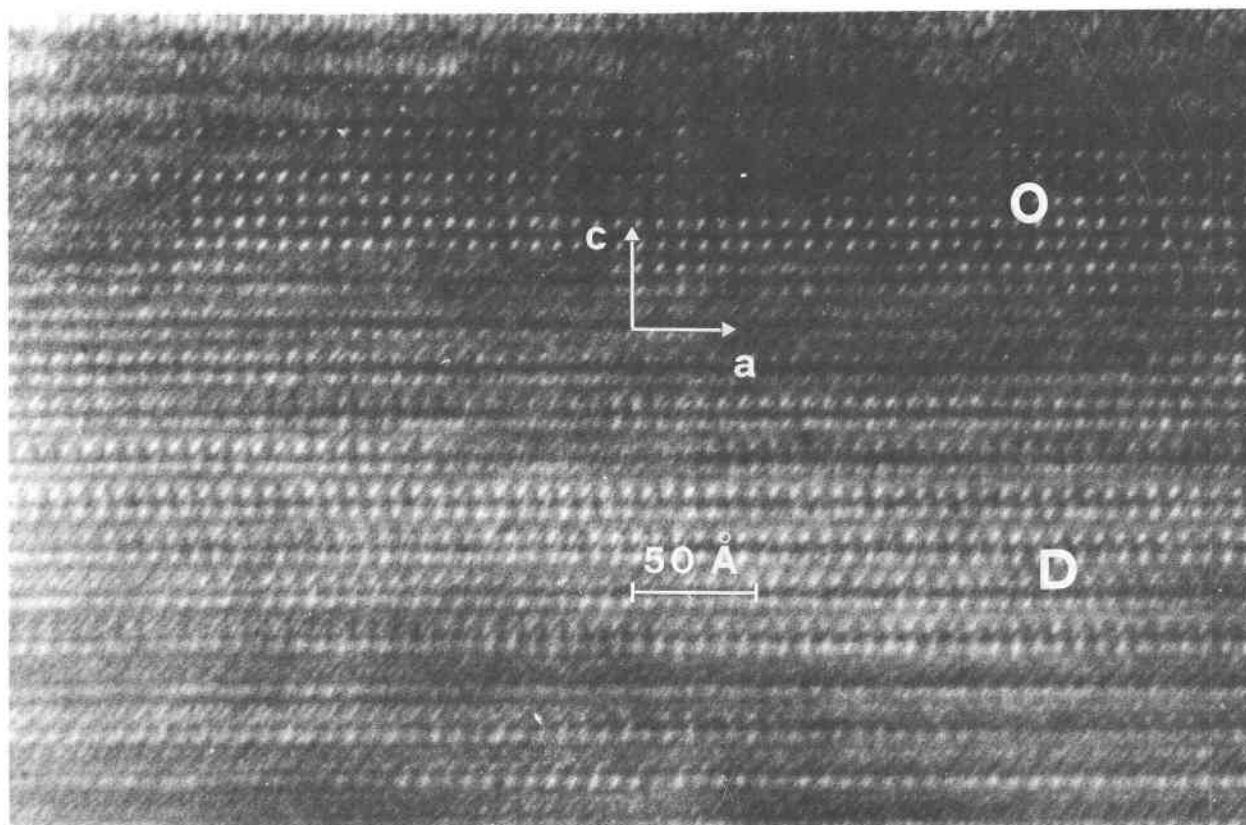


Fig. 9. Coexisting orientite (O) and doubled period, 38 Å polytype (D); poorly defined contrast is present elsewhere.

orientite, the 38 Å structure and regions with poorly defined contrast. Such an ill-defined and patchy texture is common in orientite, and, together with lamellar intergrowth, is one of the most frequent defect structures for both the Oriente and Keweenaw material.

(d) Microtubules and microvoids. Microvoids occur extensively in orientite. These empty channels are up to fractions of  $\mu\text{m}$  long and may have either subrounded or elongated cross sections, with width up to 300 Å. Clustering of voids is common (Fig. 10). Most of them are located on the borders of faulted regions and separating them from other regions that may be regular or faulted in a different fashion (Fig. 11). The formation of voids may be related to the stress field associated with the boundary between two misfitting, out of step portions of a crystal. Deformation could produce cracks and voids with elongated cross section. Circulating fluids within these channels would lead to progressive dissolution, resulting in the subrounded cross sections. The possible reprecipitation of this leached material may explain the observations of Hewett and Shannon (1921), who found that orientite crystals are usually dusted with a black opaque pigment of oxide, sometimes forming an opaque core that locally has exactly the same form as the exterior of the crystal.

### Conclusions

The combined investigation of orientite with X-rays and HRTEM led us to define a satisfactory structural model for the mineral. This model is characterized by regular alternation of ardennite-like sheets and trisilicate sheets, derived from the former by removal of two  $\text{MnO}(\text{OH})$  units, and resulting in the substitution of three tetrahedra and two octahedra by a trisilicate group and two water molecules.

The modular nature of such minerals makes other polytypic modifications plausible, and some of them are locally realized in the analyzed specimen; in particular, we observed an abundance of a polytype with doubled  $c$  period.

HRTEM investigation confirmed the common occurrence of faults in the stacking of the layers in the  $c$  direction, as well as the occurrence of polytypic modifications, in the whole family of the  $6 \times 9$  Å modular sheet structures. This happens in orientite as well as in sursassite (Mellini et al., 1984), apparently because of the small energetic differences between the possible stacking of the layers.

One major point we would stress here is the importance of HRTEM data, when associated with conventional X-ray techniques, not only in the study of fine scale dis-

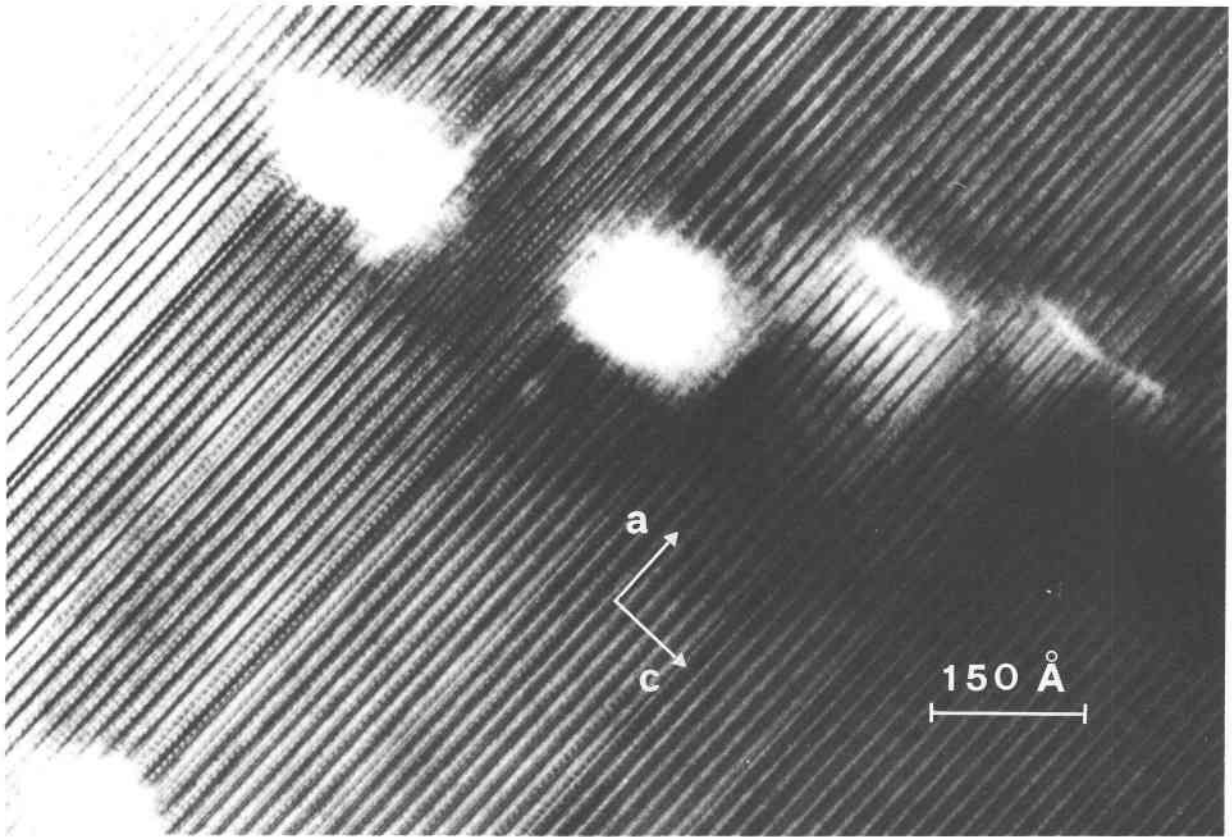


Fig. 10. Clustered microvoids in orientite as seen along [010].

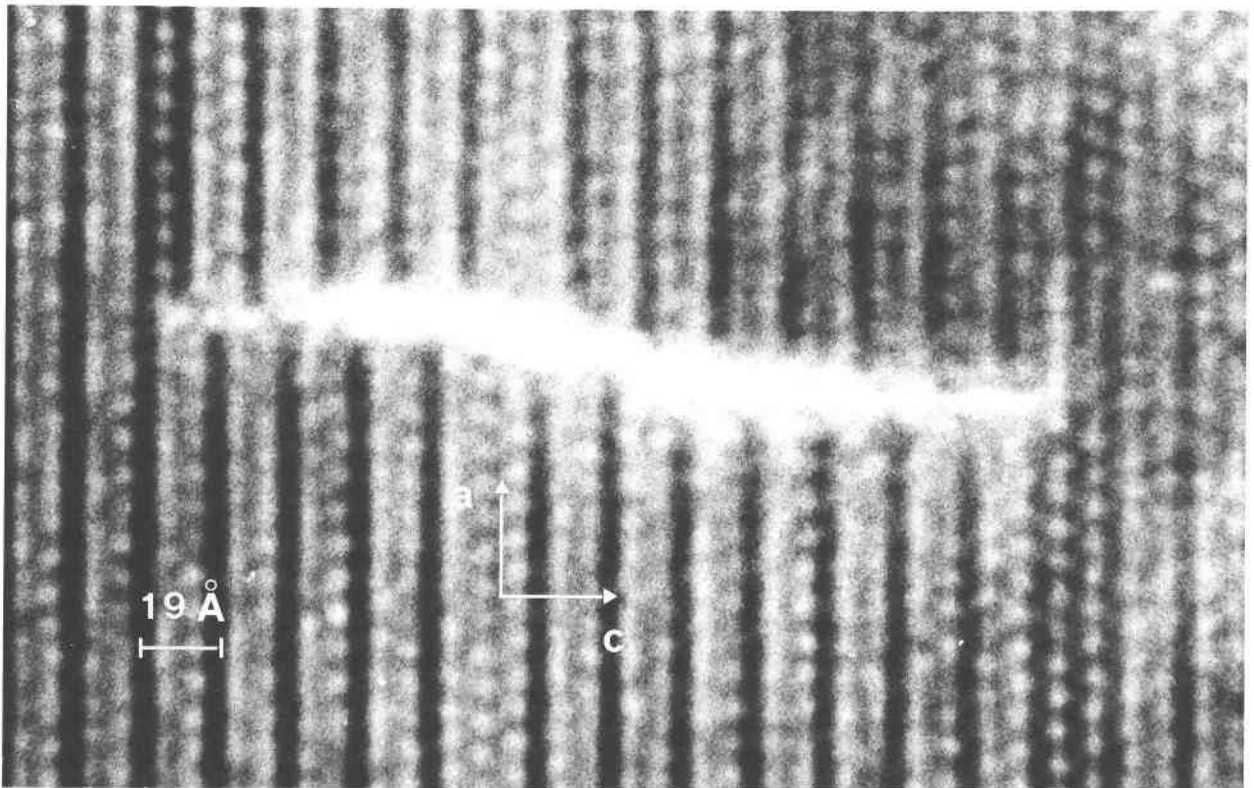


Fig. 11. Single microvoid in orientite as seen along [010].

order, but also as a further tool in crystallographic structure analysis.

### Acknowledgments

The authors would like to thank Prof. P. B. Moore for sending us a preprint of the paper "Crystal chemistry of the  $\frac{2}{3}[M_2^{3+}\Phi_2(TO_4)_2]$  sheet: structural principles and crystal structure of ruizite, macfallite and orientite" (Moore et al., 1985). P. B. Moore also provided the Keweenaw County specimens of orientite, whereas the Oriente Province specimens were supplied by Dr. E. De Michele (Museo Civico di Storia Naturale, Milano). Thanks also to Prof. G. Rossi, who helped us in the X-ray intensity data collection.

### References

- Allmann, R. and Donnay, G. (1971) Structural relation between pumpellyite and ardennite. *Acta Crystallographica*, B27, 1871–1875.
- Brown, I. D. and Wu, K. K. (1976) Empirical parameters for calculating cation-oxygen bond valences. *Acta Crystallographica*, B32, 1957–1959.
- Donnay, G. and Allmann, R. (1968)  $Si_3O_{10}$  groups in the crystal structure of ardennite. *Acta Crystallographica*, B24, 845–855.
- Hamilton, W. C. (1965) Significance tests on the crystallographic  $R$  factor. *Acta Crystallographica*, 18, 502–510.
- Hewett, D. F. and Shannon, E. V. (1921) Orientite, a new hydrous silicate of manganese and calcium from Cuba. *American Journal of Science*, 5th series, 1, 491–506.
- Kampf, A. R. and Moore, P. B. (1976) The crystal structure of bermanite, a hydrated manganese phosphate. *American Mineralogist*, 61, 1241–1248.
- Mellini, M. and Merlino, S. (1982) Order-disorder in sursassite. (abstr.) International Mineralogical Association, 13th General Meeting, Varna, Bulgaria, Abstracts of Papers, 373.
- Mellini, M., Merlino, S., and Pasero, M. (1984) X-ray and HRTEM study of sursassite: crystal structure, stacking disorder, and sursassite-pumpellyite intergrowth. *Physics and Chemistry of Minerals*, 10, 99–105.
- Moore, P. B. (1965) Cell data of orientite and its relation to ardenite and zoisite. *Canadian Mineralogist*, 9, 262–265.
- Moore, P. B., Ito, J., and Steele, I. M. (1979) Macfallite and orientite: calcium manganese (III) silicates from upper Michigan. *Mineralogical Magazine*, 43, 325–331.
- Moore, P. B., Shen, J., and Araki, T. (1985) Crystal chemistry of the  $\frac{2}{3}[M_2^{3+}\Phi_2(TO_4)_2]$  sheet: structural principles and crystal structure of ruizite, macfallite and orientite. *American Mineralogist*, 70, 171–181.
- O'Keefe, M. A. and Buseck, P. R. (1979) Computation of high resolution TEM images of minerals. *Transactions of the American Crystallographic Association*, 15, 27–44.
- Rae, A. D. (1974) The phase problem and its implications in the least-squares refinement of crystal structures. *Acta Crystallographica*, A30, 761–768.
- Sclar, C. B. (1961) Optical crystallography of orientite from Oriente Province, Cuba. *American Mineralogist*, 46, 226–232.

*Manuscript received, December 14, 1984;  
accepted for publication, August 24, 1985.*